Journal of Controlled Release 223 (2016) 75–84

Contents lists available at ScienceDirect

Journal of Controlled Release

journal homepage: www.elsevier.com/locate/jconrel

Rotating magnetic field induced oscillation of magnetic particles for *in vivo* mechanical destruction of malignant glioma

Yu Cheng [b,c,1], Megan E. Muroski [a,1], Dorothée C.M.C. Petit [d], Rhodri Mansell [d], Tarun Vemulkar [d], Ramin A. Morshed [c], Yu Han [a], Irina V. Balyasnikova [a], Craig M. Horbinski [a], Xinlei Huang [c], Lingjiao Zhang [c], Russell P. Cowburn [d], Maciej S. Lesniak [a,*]

[a] Northwestern University, Feinberg School of Medicine, Chicago, IL 60611, United States
[b] Shanghai East Hospital, The Institute for Biomedical Engineering and Nano Science, Tongji University School of Medicine, Shanghai, China
[c] The Brain Tumor Center, The University of Chicago, Chicago, IL 60637, United States
[d] Thin Film Magnetism Group, Cavendish Laboratory, University of Cambridge, JJ Thomson Avenue, Cambridge CB3 0HE, United Kingdom

ARTICLE INFO

Article history:
Received 10 July 2015
Received in revised form 27 November 2015
Accepted 16 December 2015
Available online 19 December 2015

Keywords:
Magnetic particles
Mechanical destruction
Magnetic field
Malignant glioma

ABSTRACT

Magnetic particles that can be precisely controlled under a magnetic field and transduce energy from the applied field open the way for innovative cancer treatment. Although these particles represent an area of active development for drug delivery and magnetic hyperthermia, the *in vivo* anti-tumor effect under a low-frequency magnetic field using magnetic particles has not yet been demonstrated. To-date, induced cancer cell death *via* the oscillation of nanoparticles under a low-frequency magnetic field has only been observed *in vitro*. In this report, we demonstrate the successful use of spin-vortex, disk-shaped permalloy magnetic particles in a low-frequency, rotating magnetic field for the *in vitro* and *in vivo* destruction of glioma cells. The internalized nanomagnets align themselves to the plane of the rotating magnetic field, creating a strong mechanical force which damages the cancer cell structure inducing programmed cell death. *In vivo*, the magnetic field treatment successfully reduces brain tumor size and increases the survival rate of mice bearing intracranial glioma xenografts, without adverse side effects. This study demonstrates a novel approach of controlling magnetic particles for treating malignant glioma that should be applicable to treat a wide range of cancers.

1. Introduction

The field of nanotechnology for cancer therapy has expanded drastically in the last decade with micro and nanoparticles successfully used as therapeutic or diagnostic materials [1,2]. As part of this progress, magnetic nanomaterials are now integrated in biomedical applications such as contrast agents in magnetic resonance imaging, therapeutic agents enabling magnetic hyperthermia, and drug delivery [3–6]. One advantage of these platforms is that they can induce the physical destruction of cancer cells (e.g. by hyperthermia, mechanical force), offering an alternative to molecule-based therapeutic approaches like chemotherapy agents or receptor/molecule-targeted antibodies [7–9].

Magnetic actuation via mechanic forces offers an exciting strategy to remotely control cell functions for cancer treatment [10–12]. Coupled with the magnetic materials a magnetic field can be utilized to trigger specific signaling pathways and control ion channel or surface receptor activities to actuate apoptosis within a target cell via a contactless approach [13–15]. Compared to other physical stimuli such as light and heat, magnetic field provides the distinct advantage to activate deep seated tumors in a controllable and noninvasive fashion for *in vivo* applications [16–18].

In recent years, development of novel magnetic materials via mechanical force to induce cell apoptosis has been extensively explored [19–21]. For instance, Cho et al. demonstrated a magnetic switch using zinc-doped iron oxide magnetic nanoparticle conjugated with a targeting antibody for death receptor 4 which could aggregate under a permanent magnetic field and mimic the TRAIL signaling pathway to trigger the apoptosis of zebrafish [22]. Another pathway is to transduce mechanical stimulation to targeted cellular structures in order to induce apoptosis. Zhang et al. showed that superparamagnetic iron oxide nanoparticles covalently conjugated with antibodies targeting the lysosomal protein marker LAMP1 could tear the lysosomal membrane and induce 12.45% apoptosis in INS-1 cells *in vitro* under a dynamic magnetic field [23]. Stretching cytoskeletal and actuating ion channels via mechanical forces have also been demonstrated *in vitro* for cancer destruction. Kim et al. found *in vitro* that biofunctionalized magnetic vortex microdisks could selectively transmit mechanical force to a cancer cell's membrane and induce chemical ionic signal such as calcium to

* Corresponding author at: Northwestern University Feinberg School of Medicine, 676 N. St Clair Street, Suite 2210, Chicago, IL 60611, United States.
E-mail addresses: maciej.lesniak@northwestern.edu, mlesniak@surgery.bsd.uchicago.edu (M.S. Lesniak).
[1] These authors contributed equally.

http://dx.doi.org/10.1016/j.jconrel.2015.12.028
0168-3659/

initiate programmed cell death upon exposure to an alternating field [9]. These ferromagnetic microdisks with a magnetic vortex ground state were oscillated under an alternating magnetic field with a low frequency (tens of Hz) and small amplitude (9 mt). Although these approaches provide insightful investigations for cell apoptosis activities, the gap of extending the related approach to clinical applications exists in the context of cancer treatment.

In vivo magnetic actuation of apoptosis through mechanical force is challenging for cancer treatment. It requires that majority of the magnetic particles will respond to the field to induce programmed cancer cell death in the complex biological environment. Here, our proof of principle study demonstrates the efficacy of using magnetic-vortex disk-shaped magnetic particles (MPs) in combination with a low-frequency rotating magnetic field in an animal model of malignant glioma, which carries the worst prognosis among all brain and central nervous system tumors [24]. We first examine the cellular uptake of MPs and the destruction effect of the internalized particles to glioblastoma *in vitro* under an applied magnetic field. After internalization into glioma cells, the MPs under an externally applied rotating magnetic field were shown to damage the membrane integrity of cells, leading to extensive cell death after a single 30 min treatment. *In vivo*, under the rotating magnetic field, these particles pre-incubated with glioma cells also led to a significant decrease in tumor growth as observed by increased apoptotic area in the tumor, resulting in improved survival outcomes in glioma-bearing mice.

2. Materials and methods

2.1. Materials and cell culture

The human glioma cell line U87 was purchased from the American Type Culture Collection (Manassas, VA., USA) and cultured in Dulbecco's Modification of Eagle's Medium (DMEM) (Mediatech Inc., Manassas, VA, USA), containing 2% penicillin and streptomycin antibiotic (Cellgro, Mediatech, Inc., Manassas, VA, USA) and 10% fetal bovine serum (FBS; Atlanta Biologicals, Lawrenceville, GA, USA). U87 cells constantly expressing firefly luciferase and green fluorescent protein (U87-Fluc-GFP) were established as described previously [25]. Cells were incubated with replication-deficient lentiviral vectors containing Fluc and GFP expression cassettes for 48 h. Fresh growth medium containing 1 μg mL^{-1} puromycin was added for the establishment of clonal populations. Cells were sorted by FACS to verify GFP expression. The stable Fluc expression was verified via luciferase assays.

2.2. Rotating magnet test station

The rotating magnetic field station used an NdFeB Halbach Array magnet (Bunting Magnetics Europe Ltd., Hertfordshire, UK), which produces a uniform 1 Tesla magnetic field diametrically across the central air gap. The magnet was mounted on a motor to control its rotation and the head of the mice was placed inside the central air gap. The test station was used for both in vitro and in vivo experiments. Measurement of hyperthermia was conducted with a Fluke 51 single input digital thermometer with a temperature accuracy of $\pm 0.05\% + 0.3$ °C. The experiment was conducted with complete media (DMEM + FBS) with and without the magnetic particles to observe changes during the duration of the experiment timeframe (30 min).

2.3. Animal experiments

6-week-old male athymic/nude mice weighing 18–22 g were purchased from Charles River Laboratory (Wilmington, MA, USA). Animals were cared for according to a study-specific animal protocol approved by the University of Chicago Institutional Animal Care and Use Committee. To examine the MPs cell destruction effect *in vivo*, U87-Fluc-GFP cells were incubated with MPs at 50 particles/cell ratio. A right side burr hole centered 2 mm lateral to the sagittal suture and 2 mm posterior to the coronal suture was drilled on the mouse skull. After positioning the animals in the stereotactic frame, 1×10^5 glioma cells in 5 μL PBS were injected 3 mm deep into the mouse brain. At day 4 post the glioma cell implantation, mice were randomly divided into 2 groups (n = 5 mice/group) as following: 1) untreated group as control and 2) treated group received one-hour magnetic treatment daily for 7 days. The health condition of the mice was monitored daily. During the MF treatment, the mice were kept in a DecapiCones® mouse restrainer (Braintree Scientific, Inc., MA, USA) without anesthesia. The head of the mouse was located at the center of the magnet. The magnetic field conditions were kept constant at 20 Hz rotation frequency and 1 Tesla strength for all exposures. Bioluminescence of the U87 cells due to the expressed firefly luciferase activity was imaged after intraperitoneal injection of D-luciferin (4.5 mg/animal in 150 μL of saline) at day 7, 14, 21 and 28 days post glioma cell implantation. The spatial distribution of luciferase activity within the brain was recorded using a Xenogen IVIS 200 imaging system. For the histology study, the U87 glioma-bearing mice were established by intracranially injection with 10^5 U87 glioma cells on the right hemisphere of the brain. On day 3, the mice received a second intracranial, intratumoral injection of MPs at 5×10^6 particles per animal. On day 4, animals were randomly divided into untreated group (n = 3 mice) and treated group (n = 5 mice). The treated group received the daily MF treatment for a week. The mouse brain, liver, spleen, heart, lung, kidney, large intestine, bladder and testes were collected post of the treatment. In accordance to the guidelines suggested by the University of Chicago for selecting humane endpoint in rodent studies, animal health conditions were determined through developed signs of systems of toxicity related to the treatment. The signs and symptoms include inability to would heal, hunched posture and increased respiration, weight loss (>10%), inability to reach food or water, lethargy or hemiparesis. Histological analysis for neurotoxicity was performed by a licensed neuropathologist.

2.4. Transmission electron microscopy

2.5×10^6 U87 cells were seeded into a T-75 plate. 1.25×10^8 MPs were added into the well and incubated with the cells for 24 h. Post incubation, the cells were fixed with 2% glutaraldehyde and 4% paraformaldehyde in 0.1 M sodium cacodylate buffer for 2 h. The cell pellet was washed with sodium cacodylate buffer 3 times and post fixed with 1% osmium tetroxide in 0.1 M sodium cacodylate buffer for 1 h. The cells were then washed with sodium cacodylate buffer and maleate buffer, respectively. 1% uranyl acetate in maleate buffer was applied to the cells for 1 h and then washed with maleate buffer for 3 times. The cells were dehydrated in a series of washes with increased ethanol concentration. After infiltration in a 2:1 propylene oxide:spurr resin, 1:1 propylene oxide:spurr resin and 100% spurr resin, the cell sample was polymerized overnight at 60 °C. The resin block was cut using Reichert-Jung Ultracut E microtome. The sections (90 nm thickness) were stained with uranyl acetate and lead citrate. Images were taken under 300 kV using a FEI Tecnai F30 microscope.

The sections (90 nm thickness) were stained with uranyl acetate and lead citrate to elucidate the components in the cells. Uranyl acetate was used to enhance the contrast by interaction with sialic acid carboxyl groups of lipids and proteins in addition to the nucleic acid phosphate groups of DNA. The lead citrate is used to enhance the contrast for a wide range of cellular structures due to the interactions of proteins as well as glycogens.

2.5. Evaluation of in vitro cell destruction of MPs under magnetic field

Glioma cells were seeded on 96-well plates at 1×10^4 cells per well. The cells were incubated with MPs for 1 h or 24 h. Post incubation, cells were plated into the center of the magnetic field and treated for 30 min. After 24 h, the cell destruction was quantified using MTT colorimetric

assay. 10 μL of MTT labeling reagent 3-[4,5-dimethylthiazol-2-yl]-2,5-diphenyltetrazolium bromide (Cell Proliferation Kit I (MTT), Roche Applied Sciences, Indianapolis, USA) was added into the wells and incubated for 4 h. 100 μL of 10% SDS solubilization solution was added into the wells to dissolve the purple form azan salt crystals. The plates were read on GeneMate microplate reader. 4 replicates were included for each condition and the experiments were repeated twice. In addition the scattering effects due to the MPs were accounted for by including the MPs in the control group. For the trypan blue staining, nanomagnet-loaded U87 cells were incubated with trypan blue. Cells were treated for 5 min under rotating magnetic field. For TUNEL staining, cells were stained 4 h after the magnetic field treatment. Cells were fixed with 1% paraformaldehyde in PBS at room temperature for 10 min. ApopTagplus peroxidase in situ apoptosis detection kit (S7101, Millipore, Billerica, MA) was used to detect apoptotic cells by labeling and detecting DNA strand breaks. Colors were developed by applying the AEC+ high sensitivity substrate chromogen (K3461, DAKO, Carpinteria, CA, USA). Images were taken using the Zeiss Axiovert 200 M with a Zeiss Axiocam color digital camera.

2.6. Immunohistochemistry

Brain samples were freshly frozen in Tissue-Tek® O.C.T. compound and were cut at 10 μm thickness. For cleaved caspase-3 staining, tissue slides were fixed in picric acid formalin for 10 min. Anti-cleaved caspase 3 antibody (Cell Signaling, Cat#9661, Rabbit IgG) at 1:100 was applied on tissue sections for 1 h incubation at room temperature in a humidity chamber. Following tris buffered saline (TBS) wash, the antigen-antibody binding was detected. Tissue sections were incubated with biotinylated anti-rabbit IgG (1:200, BA-1000, Vector laboratories) for 30 min at room temperature. The antigen-antibody binding was detected by Elite kit (PK-6100, Vector Laboratories) and diaminobenzidine (DAB) (DAKO, K3468) system. Tissue sections were briefly immersed in hematoxylin for counterstaining and were covered with cover glasses. For TUNEL staining, cryosections were fixed in 1% paraformaldehyde in PBS at room temperature for 10 min with post fixation by cold ethanol: acetic acid (2:1) solution at −20 °C for 5 min then washed extensively by PBS. After immersion in 3% H_2O_2 for 5 min, sections were washed by PBS and incubated in the equilibration buffer for 20 min. Sections were subsequently incubated with the working strength terminal deoxynucleotidyl transferase (TdT) enzyme in a humidified chamber for 60 min at 37 °C then with the stop buffer at the same condition for 5 min. After washing by PBS, the anti-digoxigenin peroxidase conjugate was applied to the sections and incubated at the above condition for 30 min. Colors were developed by applying the AEC+ high sensitivity substrate chromogen for 2 min at room temperature and counterstained by hematoxylin. Upon staining, the whole slide was scanned by the Cri Pannoramic scan whole slide scanner and analyzed with the Pannoramic Viewer 1.14.53.0 software. The non-tumor brain area and tumor area were exported respectively as individual images by the above software and TUNEL positive stained cells were counted using an image processing software. The H & AEC color deconvolution function of ImageJ was applied to each image and the orange/red colored AEC positive TUNEL stained cells were counted as the apoptotic cells while the number with the blue colored hematoxylin cells was counted as the total number of cells to calculate the TUNEL positive index of each sample.

2.7. ICP-MS

Tissues from the nanomagnet injected glioma-bearing mice were collected. Animals injected with PBS were included as the control. The tissues were digested in concentrated nitric acid and the resulting solutions were diluted in 2% HNO_3 solution for ICP-MS analysis based on Au content. Three replicates were used per condition.

2.8. Image J analysis

To determine the number of MP within the cells, twenty 20× images were acquired and analyzed on Image J software. The MPs have negative contrast in the field of view and are easily distinguishable from the cells. The images were converted to a binary image and the total area of the MP was analyzed to respect of the number of cells in the field of view. The μm/pixel of the MP was determined by the average area of the MP. Each cell count was completed in triplicate.

2.9. Flow cytometry

7-amino-actinomycin D (7-AAD) was used to measure the cell viability of the cells. After MF treatment the cells were trypsinized and 2×10^5 cells were washed three times and resuspended in PBS, the cell suspension was labeled according to the manufacturer's instructions. After 15 min incubation, the cells were washed and detected (10,000 events) using the LSR IIB and the data was analyzed using Flow-Jo software.

2.10. Statistical analysis

All statistical analyses were performed using Graphpad Prism 4 (GraphPad Software Inc., San Diego CA). The sample size for each group was ≥3 and numerical data was reported as Mean ± SEM. Comparisons between two groups were conducted using Student's t test, and differences between more than two groups were assessed using ANOVA with Tukey's post hoc test. Kaplan–Meier survival curve was generated and log rank test was applied to compare survival distributions. All reported p values were two-sided and were considered to be statistically significant at $^{*}p < 0.05$, $^{**}p < 0.01$, $^{***}p < 0.001$.

3. Results and discussion

3.1. MPs induce glioma cell destruction under a rotating magnetic field in vitro

The 2 μm diameter disk-shaped MPs were fabricated by the thermal evaporation of 5 nm Au/60 nm permalloy ($Ni_{80}Fe_{20}$)/5 nm Au onto resist pillars made by optical lithography [9,26]. Under zero applied magnetic field, the magnetization of the nanomagnet forms a vortex leading to zero net moment (Figs. S1, S2), minimizing aggregation due to particle–particle interactions [27]. In addition, synthesis through optical lithography results in a uniform composition, size and shape distribution. The particles are a two-dimensional structure designed a with spin-vortex ground state leading to zero next moment to minimize the aggregation due to particle–particle interactions and have a higher saturation magnetization to induce a higher mechanical force as compared to other particles used for magnetization therapies [28].

Under large applied magnetic fields, such as the 1 T field used in these experiments, the magnetic vortex is expelled leading to a particle with a saturated in-plane moment as shown in Fig. 1A. The torque on the MP is the cross product of the magnetization by the applied field. Since the magnetization can rotate freely in the plane of the particle, only the field perpendicular to the plane of the MPs applies a torque to rotate the particles. In the case of the rotating field applied here, the torque acts to align the plane of the particles with the plane of the rotating magnetic field, as schematically shown in Fig. 1A.

In order to test the *in vitro* toxicity, U87 human glioma cells were loaded with MPs at a ratio of 50 particles per cell (Fig. 1B). After 24 h of incubation, nearly 100% of U87 glioma cells were observed to have taken up MPs, with no apparent alteration in cellular morphology.

After exposure to a rotating magnetic field (MF treatment) of 1 Tesla at 20 Hz for 30 min, the treated cells were visibly disrupted with cellular fragments observed throughout the field of view (Fig. 1B). This suggests that the MPs can create a mechanical force that disrupts the cellular

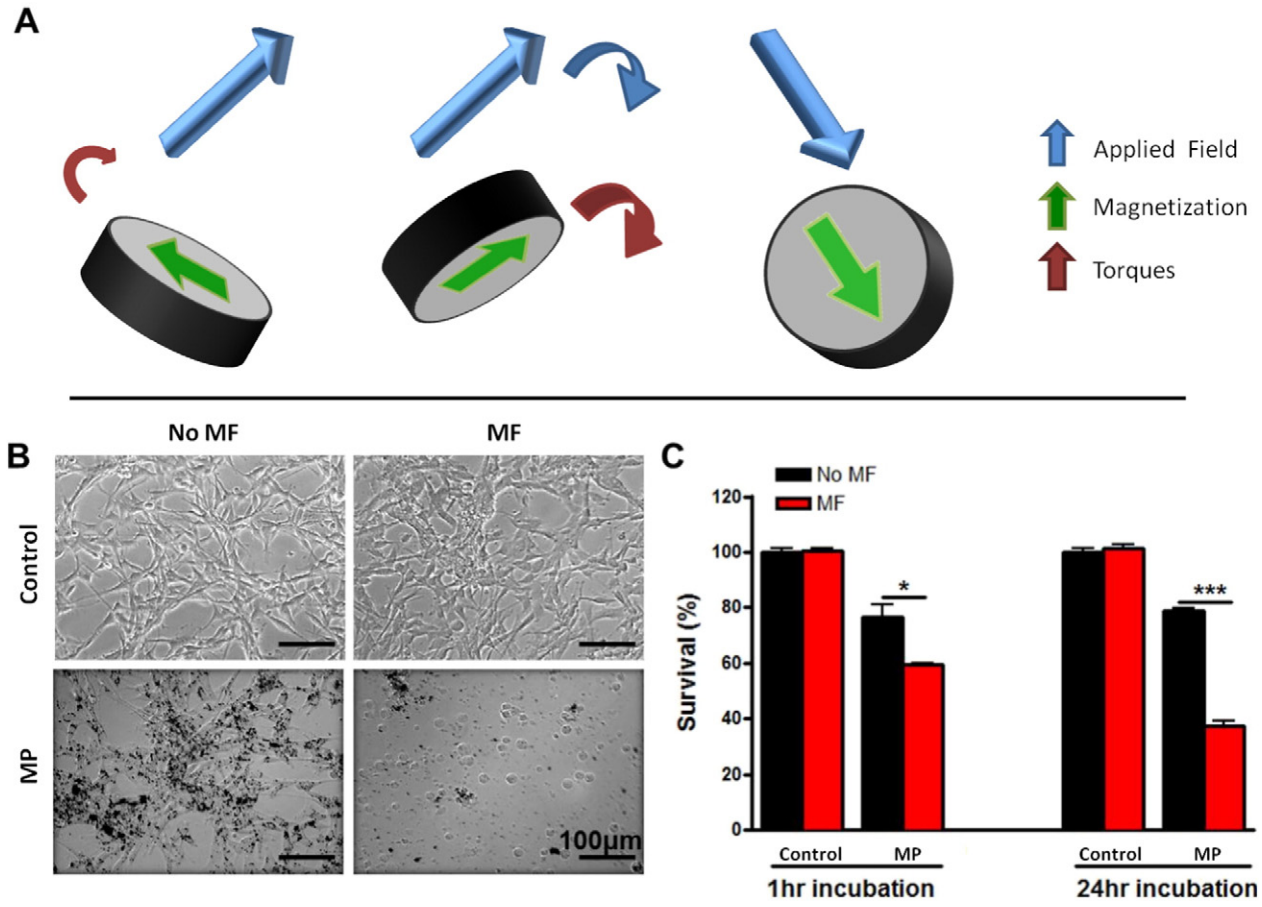

Fig. 1. *In vitro* cell destruction using MPs under a rotating magnetic field (MF). (**A**) Schematic of one of our MPs under a rotating MF. (**B**) Optical images of U87 glioma cells with (MF) and without (no MF) MF treatment (1 Tesla at 20 Hz for 30 min). Cells were treated with either growth media (control) or MPs at 50 particles per cell for 24 h. Scale: 100 μm. (**C**) Quantification of the U87 cells viability after incubation with the MPs for 1 h and 24 h or not, and after MF treatment or not. Data are presented as Mean ± SE. * $p < 0.05$, *** $p < 0.001$ (Student's t test).

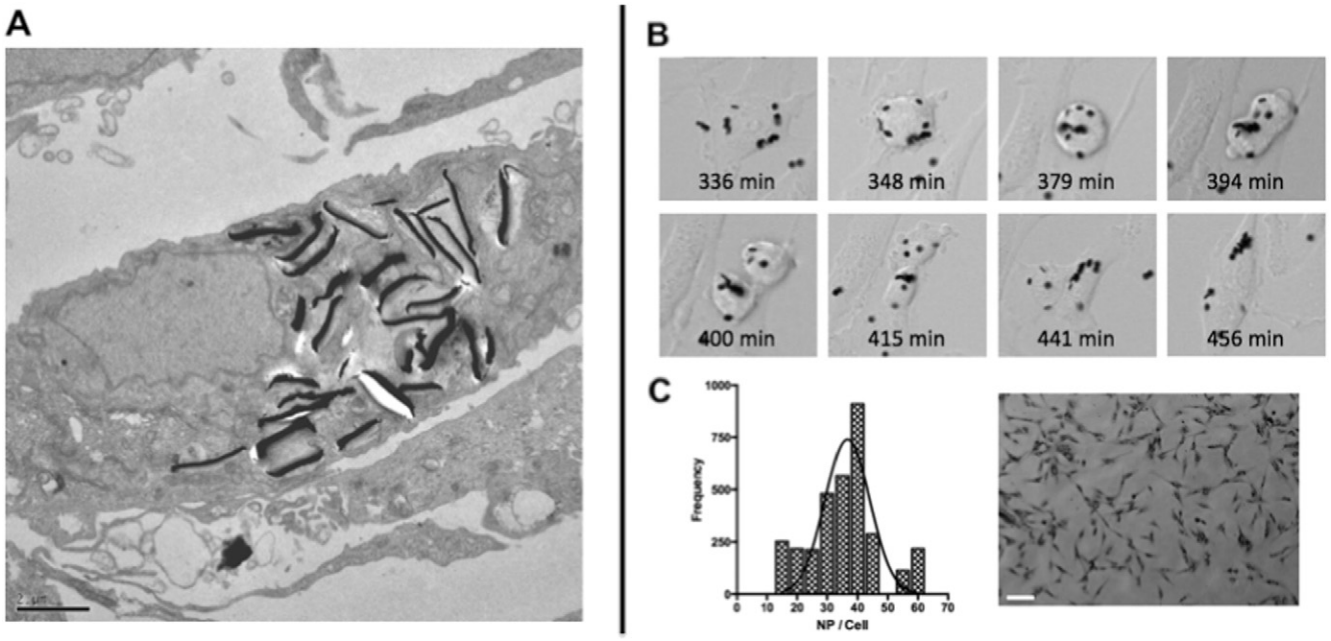

Fig. 2. MPs can be internalized into glioma cells. (**A**) TEM image of U87 cells after 24 h incubation with MPs loaded at an average 50 particles per cell. Scale Bar 2 μm (**B**). Uptake and distribution of MPs into U87 cells during mitosis. **(C)** Normal density function of the number of particles per cell, with a peak at 38.9 particles per cell (3000 cells analyzed) and representative 10× image, scale bar 100 μm.

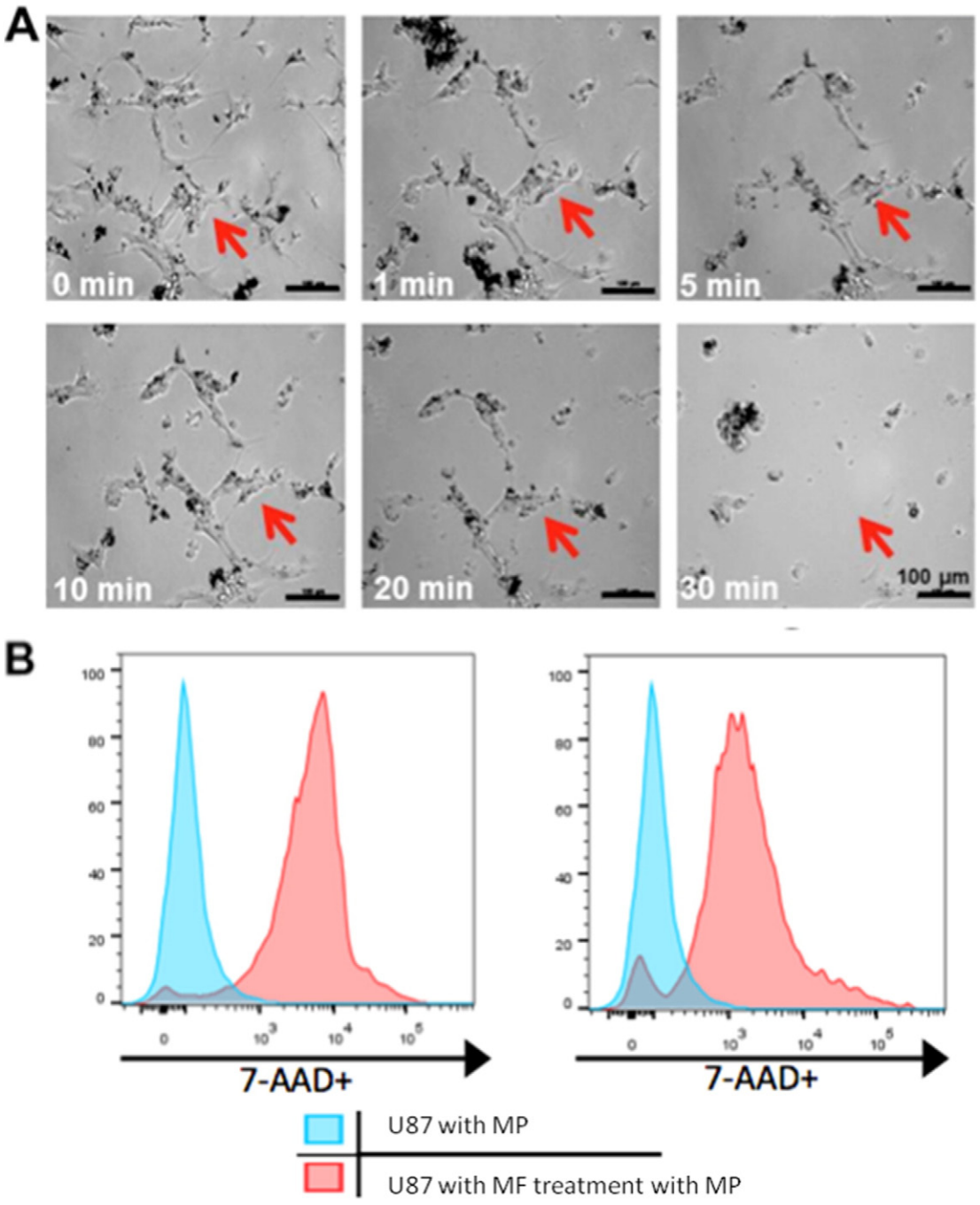

Fig. 3. MPs compromise the membrane integrity of cancer cells under magnetic field. (**A**) Optical images of nanomagnet-loaded U87 cells after MF treatment. Cells were incubated with MPs at 50 particles per cell for 24 h. Images were taken from 0 min to 30 min post magnetic field treatment (1 Tesla, 20 Hz). The same area was monitored as indicated as the red arrow. (**B**) Flow cytometry analysis of cells (10,000 events) 5 min and 30 min after MF treatment. The cells compared with the controls that were incubated with particles show 89.3% and 87% 7-AAD staining respectively.

integrity. This cell destruction effect was quantified using MTT assays (Fig. 1C). With 1 h incubation, about 40% of the glioma cells were destroyed after the MF treatment. After 24 h incubation, over 60% of the cells were destroyed. We checked that the magnetic field alone had little effect on glioma cell viability (control + MF experiment in Fig. 1C). In addition, the stability of the MPs was observed with transmission electron microscopy (TEM) before and after cellular experiments and no change in shape or structure was determined (Fig. S3). In Supporting Fig. S4 we determine that there is no significant hyperthermic reaction from the rotation of the particles. Media with serum with and without MP in the presence of a magnetic field did not demonstrate significant differences in temperature over the treatment time measured. Our controlled system demonstrates the low risk associated with high thermal temperatures and therefore does not require monitoring of the temperature of the tumor and surrounding tissues.

3.2. MPs can be internalized into the glioma cells and induce apoptosis under a rotating magnetic field

In order to further understand how the MPs interact with cells, TEM was applied to provide insight to the intracellular localization of these particles. The majority of MPs were internalized into U87 cells without disturbing the cell membrane or morphology after 24 h incubation (Fig. 2A).

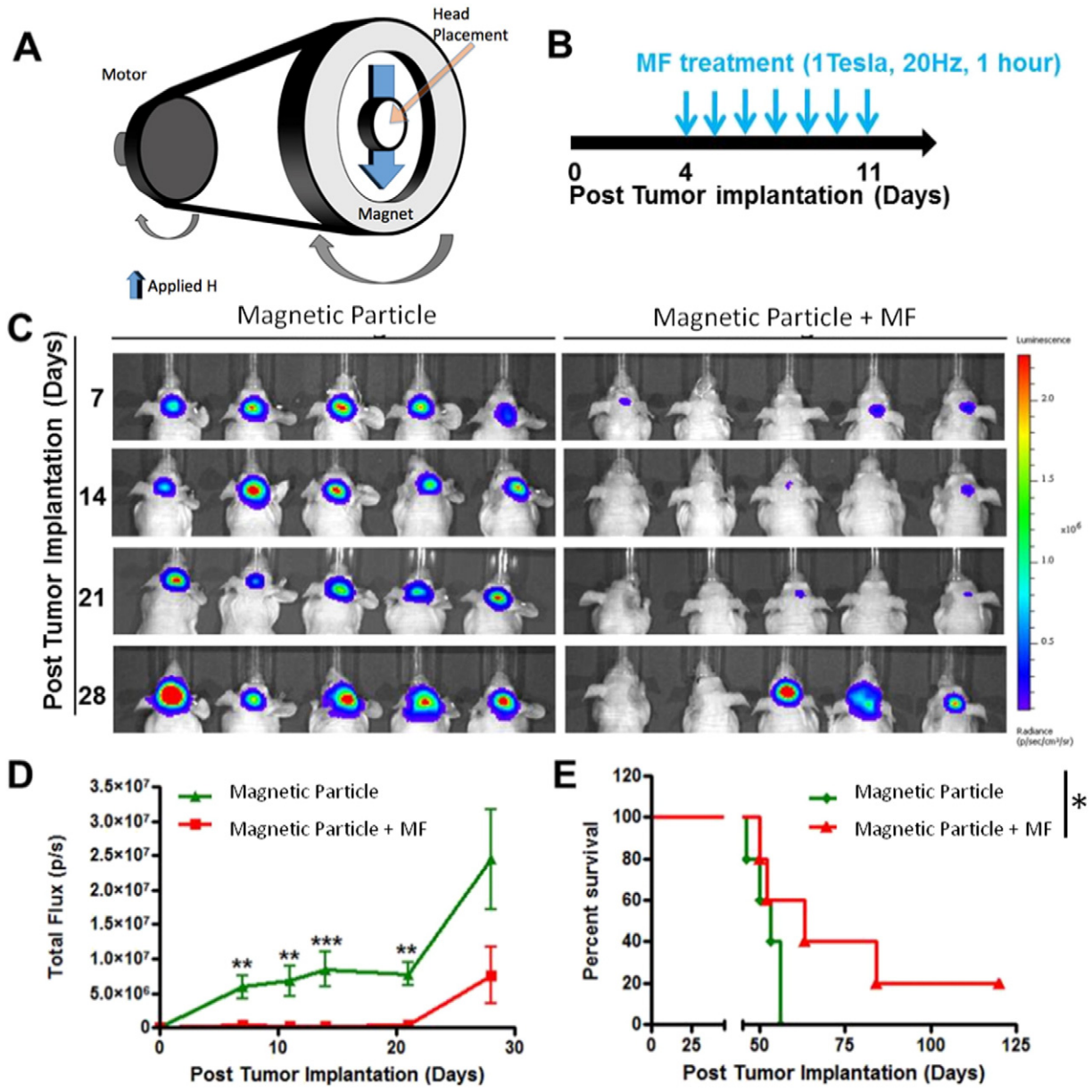

Fig. 4. *In vivo* therapeutic efficacy of the MPs under rotating magnetic field. (**A**) The rotating MF setup for animal experiments. (**B**) *In vivo* design of animal studies. The U87 cells were pre-incubated with MPs for 24 h and implanted in the mouse brain. At day 4 after tumor implantation, animals received 1 h long daily exposures to the MF for 7 days starting. (**C**) *In vivo* bioluminescence images of the glioma-bearing mice with MPs. MPs loaded U87 glioma cells were labeled with firefly luciferase. Bioluminescence images were taken at day 7, 14, 21 and 28 days post tumor implantation. (**D**) Quantification of the tumor bioluminescence signal over 4 weeks (n = 5 mice per group). Data are presented as Mean ± SE. ** $p < 0.01$, *** $p < 0.001$ (Student's t test). (**E**) Kaplan–Meier survival curve of the mice with and without MF treatment. * $p < 0.05$ (log rank test).

The MPs accumulated extensively within cells, mostly near the nuclear membrane. A few MPs were found near the cell surface. Although the surface of the MPs was not functionalized, it is thought that due to the high binding affinity between the gold surface of the MPs and biomolecules such as proteins with carboxylate, amine and thiol groups, the interaction between the MPs and the plasma membrane was promoted, which induced the internalization of MPs into the glioma cells. Interestingly the particles in TEM are all oriented perpendicular to the axis, in contrast to Fig. 2B, suggesting that the particles may have inadvertently been exposed to a low magnetic field, during the fixation process. The internalized MPs provided a direct interaction to the glioma cells and played a significant role for cell destruction under magnetic field.

To observe the internalization of the MPs in real time, MPs were incubated with U87 cells and an image was collected every minute for 24 h (Supplemental Video). The MPs are clearly taken up by the cell and are distributed during mitosis, indicating that the MPs can be further distributed within the cellular population (Fig. 2B). Next, we wanted to determine the number of MPs internalized by the cells, with a 50:1 MP to cell loading ratio. The cells were allowed to incubate with the MPs for 24 h and subsequently analyzed by Image J analysis, the representative figure on the right represents a particle loading of n = 20 (Fig. 2C). We were able to determine that the cells had taken up an average of 76% of the MPs, or 39 MPs/cell. This does not account for the redistribution of MPs due to the division of cells in the 24 h incubation period, and therefore may be a slightly lowered uptake figure of MPs by the cells.

To study the cell destruction mechanism, U87 cells incubated with MPs for 24 h were monitored under an optical microscope during MF treatment (1 Tesla, 20 Hz) (Fig. 3A). After 1 min of exposure to the

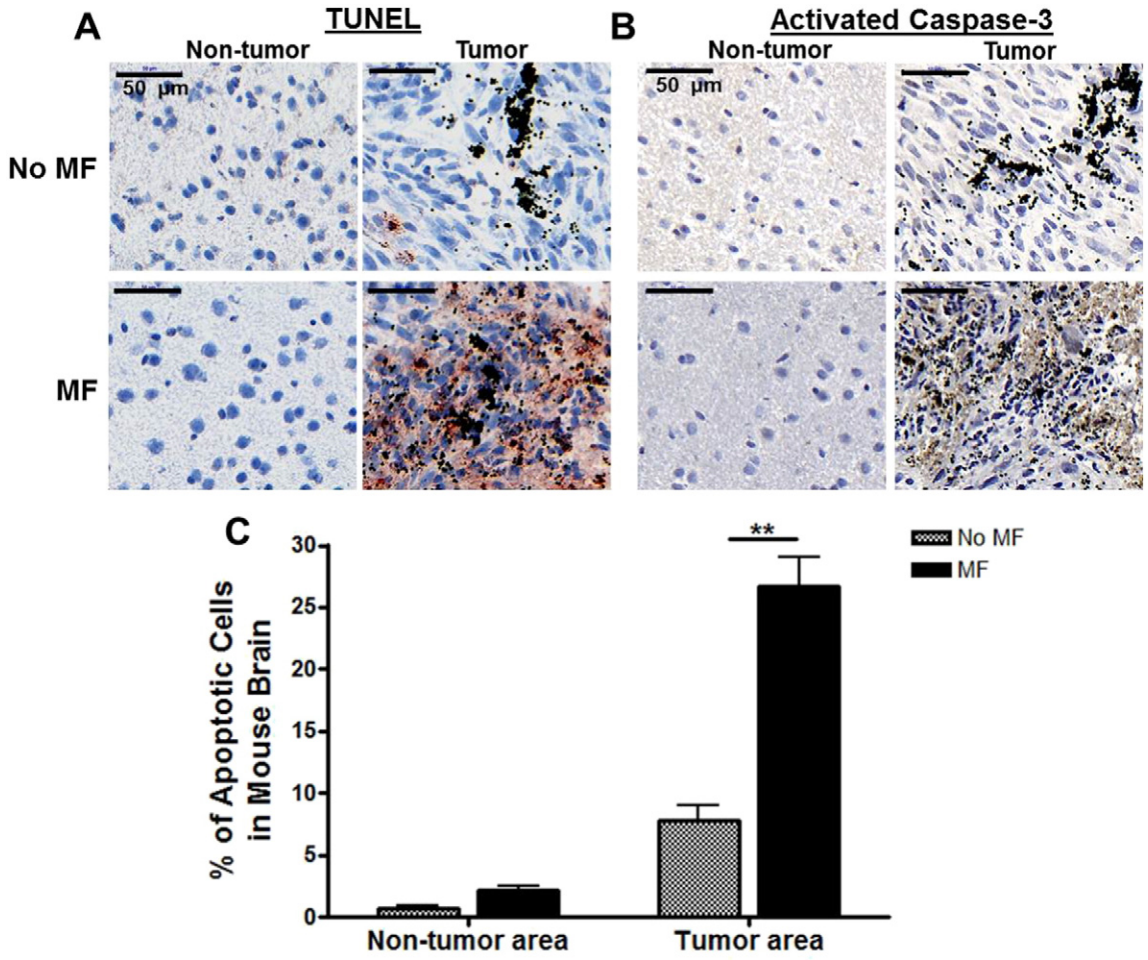

Fig. 5. Local administration of MPs induces apoptosis in the brain tumor after MF treatment. TUNEL staining (**A**) and activated caspase-3 staining (**B**) of mouse brain tissues after local administration of MPs in the U87 glioma-bearing mice. The MPs were injected intratumorally at day 3 after tumor implantation. Daily 1 h MF treatment started on day 4 post intratumoral injection of MPs and continued for 7 days. MPs are seen as black dots in the tissue. Apoptotic cells were stained with orange/red color for TUNEL staining and brown color for the activated caspase-3 staining. (**C**) Quantification of the apoptotic cells in the brain tissues. Data are presented as Mean ± SE (n = 3 mice for no magnetic field treated group, n = 5 mice for magnetic field treated group).

field, cells were already damaged and started to change shape. A number of cells even detached from the cell culture dish suggesting that the MF treatment made the cells less adhesive. The cells were allowed to recover for 24 h before MTT analysis (Fig. S5). This phenomenon was more and more pronounced with increased MF treatment duration. Apoptosis is a form of highly organized and programmed cell death process and inactivation of this process has been associated with the development of cancer and autoimmune diseases [29]. The observed cell morphological change and increased number of positive trypan blue stained cells suggests that the MPs could effectively induce cell death under MF treatment, in agreement with our previous study. Previously, we showed that membrane-bound ferromagnetic disks can stretch the cell membrane, open mechano-sensitive channels and trigger apoptosis in an oscillating field. Here, we found that internalized MPs could induce apoptosis via mechanical forces under the rotating field. Compared to the membrane-bound disks, the internalized MPs could damage the cells more efficiently as shown in Fig. 1B. The optical images suggest that the internalized MPs were responsive to the field treatment and caused the physical destruction to the cancer cells.

In addition to observed cellular destruction, cells were stained with 7-aminoactinomycin (AAD), a common fluorescent indicator of cell viability, after 5 min and 30 min of MF treatment and analyzed through flow cytometry. As shown in Fig. 3, the cells compared to controls incubated with particles show 89.3% and 87% 7-AAD staining for 5 min and 30 min respectively. This result indicates that the majority of cells are immediately affected by the MF treatment. In addition, in order to confirm the previous results, a trypan blue exclusion test was used to evaluate the integrity of the cancer cell membrane (Fig. S6). Only dead cells or cells with damaged membrane allow the dye to be internalized and stained with blue color. In the absence of MF treatment, only 1.7% of MP-loaded U87 cells showed positive staining, suggesting the uptake of MPs did not alter the integrity of the membrane. After a 5 min MF treatment, followed by a 24 h period before staining, to ensure all cell death mechanisms had completed, approximately 26% of the cells were positively stained (Fig. S6), indicating that in the presence of the rotating MF, the MPs created a mechanical force strong enough to compromise the integrity of a cell's membrane. Terminal deoxynucleotidyl transferased UTP nick end labeling (TUNEL) assay was used for detecting DNA fragmentation that results from late apoptotic cascades. After 4 h of treatment, 33% of cells were stained positive after TUNEL staining (Fig. S6). Some cells showed morphological change but no TUNEL staining, which could be attributed to a necrotic cell death process due to the strong mechanical disruption of the cell structure. Furthermore, no significant TUNEL positive cells were observed in the untreated cells (MPs and no MF) or cells only treated with the field (control + MF).

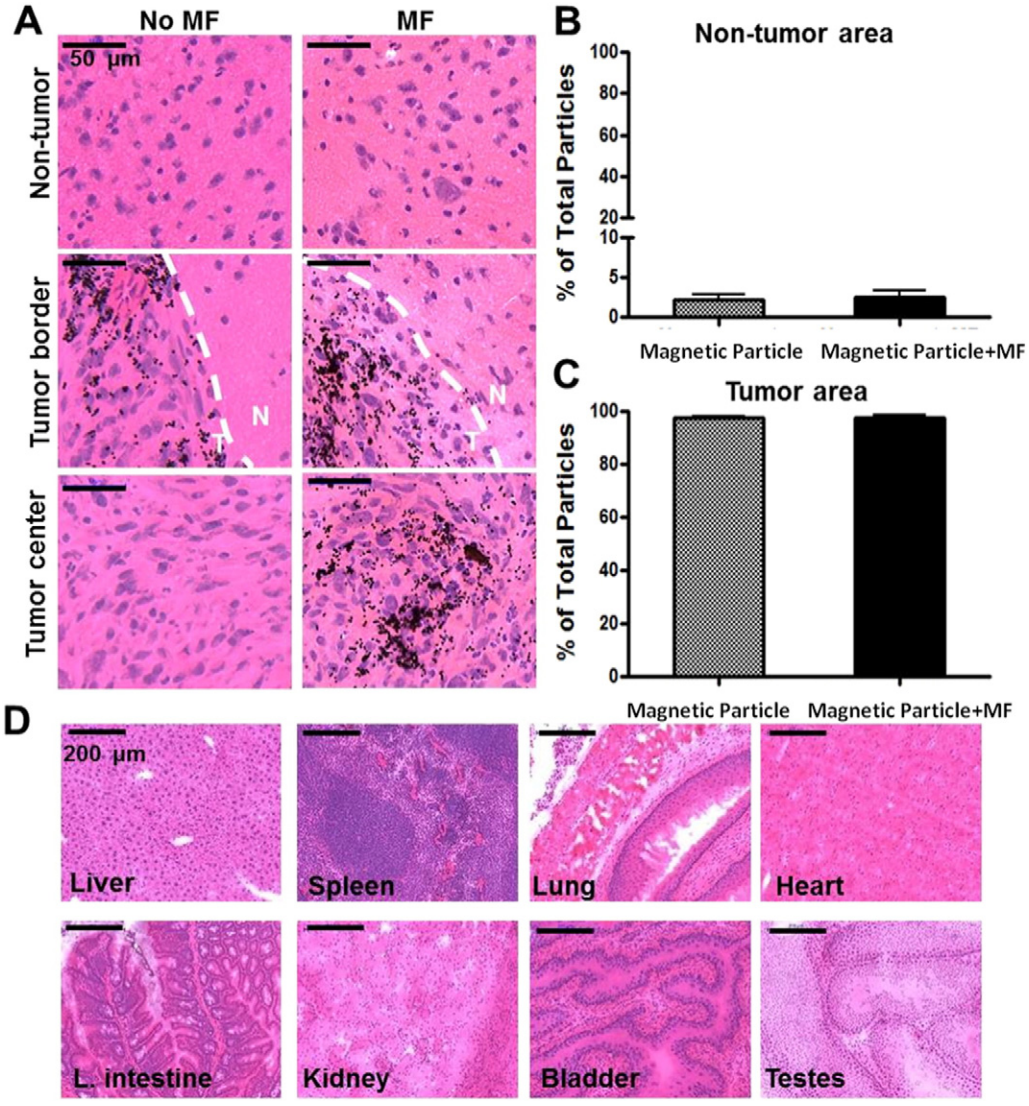

Fig. 6. Local administration of MPs shows tumor-accumulation. (**A**) Distribution of the MPs in the mouse brain after local administration in the U87 glioma-bearing mice with and without MF treatment. After MF treatment, the brain sections were stained with H&E. MPs are seen as black dots in the tissue. Quantification of the MPs distribution in the non-tumor (**B**) and tumor area (**C**). MPs are mainly found in the brain tumor. Data are presented as Mean ± SE (n = 3 mice per group). **(D)** Biodistribution of the MPs after MF treatment. Mouse tissue samples including liver, spleen, heart, lungs, large intestine, kidney, bladder and testes were stained with H&E. No MPs were found in these organs.

3.3. MPs show anti-tumor effect in vivo under rotating magnetic field

Current approaches in brain tumor treatment offer resection of the tumor among radiation and chemotherapies. Particle treatments for glioma often rely on various targeting techniques, including but not limited to the enhanced permeability and retention, often referred to at the EPR effect. Unfortunately this leaves very little focus on potential treatments that could be used in combination with current techniques. Therefore, to evaluate the anti-tumor effect of the MP platform, athymic nude mice were implanted with U87 glioma cells that had been incubated for 24 h prior to injection with MP sat a 50:1 MP to cell ratio and had not received magnetic field treatment. In order to receive the MF treatment, the head of a mouse was placed inside the gap of a rotating 1 T Halbach magnet assembly, shown schematically in Fig. 4A.

The treatment group received a daily one-hour exposure to a 20 Hz rotating 1 T magnetic field for 7 days (Fig. 4B). The U87 cells used for the study were previously labeled with the firefly luciferase gene in order to track tumor growth via bioluminescence imaging quantitatively (Fig. 4C) [30]. The control group, MPs without MF treatment, showed sustained growth of the intracranial tumors, in contrast to the treatment group, which exhibited tumor regression by day 7, (4 days into MF treatment). We observed that by two weeks 40% of the treatment group had no significant tumor signal as measured by total flux, and 60% of the group had significantly lower luciferase signal compared to the control group (Fig. 4D). Significantly, 21 days after tumor implantation, the treatment group exhibited little luciferase signal in 60% of the mice indicating that tumor growth was successfully controlled. Furthermore, by day 28, 40% of the treatment group did not show an obvious tumor signal, indicating that tumor growth was successfully inhibited by the treatment (Fig. 4D). The treatment group had a longer median survival time (63 days) compared to the control group (56 days) after one treatment cycle (Fig. 4E), which is consistent with the bioluminescence imaging results. In addition, a long-term survival benefit was observed in 40% of the treatment group, while the entire control group had died by day 56, suggesting successful tumor regression after the treatment.

The reduced tumor size and long survival rate of the treated mice suggest that the MPs can damage the cancer cells *in vivo* under MF treatment. We have successfully demonstrated that in the simplified model

in which MPs are incubated with the glioma cells prior to implantation, the MF treatment successfully lengthens the life expectancy of mice. However, in order to move closer to a more realistic therapeutic model, we also explore the effect of locally injecting the MPs inside an established tumor.

3.4. Intratumoral MPs induces apoptosis

To better understand the *in vivo* destruction mechanism in a therapeutic model, MPs were intratumorally injected, and brain tissues were collected post treatment and analyzed via histology studies. U87 cells were intracranially injected 4 days prior to MF treatment. 24 h prior to MF treatment, MPs were intratumorally injected with a ratio of 50:1 MP to injected cell. The treatment group was treated with a rotating magnetic field of 1 T at 20 Hz for 30 min over a period of 7 days. In the control group (MPs without MF treatment) apoptosis in either the normal brain tissue or the cancerous tissue was not observed. This was shown by a TUNEL staining assay (Fig. 5A) where a nonsignificant number of TUNEL positive cells (stained with orange color) were present.

The treatment group (MPs with MF treatment), conversely, showed an increase in intratumoral apoptosis, as demonstrated by the increase of positive stained cells. No significant TUNEL positive cells were observed in the non-tumor area (normal brain) in either group (Fig. 5C), suggesting that the MPs induce apoptosis in the tumor area only. Additionally the apoptotic area closely overlapped the distribution of MPs. TUNEL positive cells increased to 26% in the treatment group tumor tissue in comparison to 7% in the control group tumor tissue (Fig. 5C).

The apoptosis pathway was further verified via examination of stained cleaved caspase-3, an activated form of caspase-3 which is a late stage apoptotic marker (Fig. 5B). The brain tissue adjacent to the TUNEL stained slide was collected and stained. Similar to the TUNEL results, the cleaved caspase-3 signal, as shown by the brown stain, was observed only within the tumor area with the treatment group, suggesting that MPs without MF treatment do not cause apoptosis. In summary, our results suggest that the movement generated by MPs under a rotating magnetic field resulted in enough mechanical force to damage brain tumor cells *in vivo* and trigger the apoptotic pathway.

3.5. Biodistribution of MPs after local administration

To further study the biodistribution of the MPs in a therapeutic model, brain tissue was stained via hematoxylin and eosin (H&E) staining (Fig. 6A). The majority of the particles are found in the tumor and near the injection site 7 days after intratumoral administration of MPs (Fig. 6B and C), which is expected due to the size of the MP. Few MPs were found in the non-tumor area, indicating that MPs are taken up by malignant cells and remain in the tumor tissue rather than in the normal tissue. To verify that the MPs did not cause toxicity to the normal tissue, a full histologic evaluation, in the brain parenchyma outside the tumor, including the cerebrum, deep gray nuclei, hippocampus, and cerebellum, showed no difference between MD with or without MF treatment. There were no changes in neuronal or glial morphology, no evidence of neuronal toxicity (*e.g.* apoptosis or single-cell necrosis), no white matter vacuolation, no reactive astrocytosis or microglia, no ependymal disruption, no vasculopathy, and no inflammatory infiltrates. Also, there was no evidence of iron particle accumulation in areas outside the tumor in either treated or untreated brains. In addition to the histologic analysis, we observed that administration of the MPs in the brain (without tumor) resulted in stable body weight and health conditions in the period of 210 days post the injection. Many gliomas have a broken blood brain barrier and it is important to verify that the MPs not distribute throughout other organs. Finally, histological examination (Fig. 6D) and ICP-MS showed that no particles were found in mouse organ tissues including liver, spleen, heart, lungs, large intestine, kidney, bladder and testes after treatment, suggesting that the MPs could not be easily cleared from the brain.

4. Conclusion

Treatment of malignant gliomas represents one of the most challenging clinical problems in oncology. Despite the large array of commonly available cancer treatment, such as surgical resection, adjuvant radiotherapy and chemotherapy with temozolomide, the prognosis of patients with malignant gliomas remains poor. Therapeutic resistance of malignant glioma cells is a major hurdle, which results in tumor persistence and recurrence following treatment [31]. The present magnetic field mediated treatment offers the unique advantage that it can non-invasively and remotely induce apoptosis *via* mechanical force of MPs for treating malignant glioma. Magnetic fields can safely be used therapeutically at low frequencies to penetrate the human body, including the head, without damaging the biological tissues and can be operated in a time selective and spatially constrained manner, as the interaction is mediated by the particles. It has been reported that superparamagnetic iron oxide nanoparticles generate heat upon exposure to a high-frequency alternating magnetic field (100–500 KHz) and cause cell death through hyperthermia [5,32]. However, placing the nanoparticles inside the tumor is not enough to restrict the hyperthermic effect to cancerous tissue without affecting normal tissue [33]. For superparamagnetic iron oxide nanoparticles that use heat dissipation, the normal tissue that is near the nanoparticle treated tumor may be affected. Our system utilizes mechanical destruction *via* MPs under a rotating magnetic field is localized to the cells containing the MPs. In addition, due to the low-frequency field (20 Hz) applied for the study, no heating effect is expected under the rotating magnetic field as our magnetic field frequency is on average 10,000 orders lower than that of alternating magnetic field, which tends to be in the kHz–MHz range. Furthermore, a recent article by Zhang and colleagues demonstrated that magnetic particles at 20 Hz did not increase the temperature in their dynamic magnetic field [23]. Our *in vitro* studies show that the majority of MPs can be internalized into glioma cells and create enough force to damage the integrity of a cancer cell's membrane, leading to loss of viability. Up to 89% of non-viable cells were induced *in vitro* after magnetic field treatment.

In summary, this study has demonstrated a unique approach for *in vivo* destruction of glioma cells using the oscillation of MPs under a low-frequency rotating magnetic field. Under the rotating magnetic field, the internalized MPs can efficiently damage the cell membrane *via* mechanical force and promote programmed cell death *in vitro* and *in vivo*. Magnetic field treatment successfully reduces the brain tumor size and prolongs the survival rate of mice bearing intracranial glioma xenografts previously incubated with MPs without adverse side effects. Due to these encouraging *in vivo* anti-tumor effects, future directions include optimization of treatment dose and cycles, long-term safety evaluation, and controlled delivery in order to combine other therapeutic modalities and applications to treat a wide range of cancers.

Abbreviations

MPs	permalloy magnetic particles
GBM	glioblastoma
MF	magnetic field
TEM	transmission electron microscopy
7-AAD	7-aminoactinomycin
TUNEL	transferased UTP nick end labeling
H&E	hematoxylin and eosin
DMEM	Dulbecco's Modification of Eagle's Medium
FBS	fetal bovine serum
TBS	tris buffered saline
DAB	diaminobenzidine
TdT	deoxynucleotidyl transferase

Description of MPs, magnetic response of MPs, Stability of MPs, time dependent optical images of MF, Trypan Blue and TUNEL staining in vitro is available free of charge *via* the Internet at http://pubs.acs.org. Supplementary data associated with this article can be found in the online version, at http://dx.doi.org/10.1016/j.jconrel.2015.12.028.

Author Contributions

The manuscript was written through contributions of all authors. All authors have given approval to the final version of the manuscript.

Funding Sources

This work is supported by the National Institute of Neurological Disorders and Stroke R01NS077388 to MSL.

Acknowledgment

We thank Yimei Chen at the Electron Microscopy Core Facility of University of Chicago for the assistance in TEM image analysis.

References

[1] M. Ryvolova, J. Chomoucka, J. Drbohlavova, P. Kopel, P. Babula, D. Hynek, V. Adam, T. Eckschlager, J. Hubalek, M. Stiborova, J. Kaiser, R. Kizek, Sensors (Basel) 12 (2012) 14792–14820.
[2] R. Sensenig, Y. Sapir, C. MacDonald, S. Cohen, B. Polyak, Nanomedicine (London) 7 (2012) 1425–1442.
[3] M.L. Wegscheid, R.A. Morshed, Y. Cheng, M.S. Lesniak, Expert Opin. Drug Deliv. 11 (2014) 957–975.
[4] K. Maier-Hauff, F. Ulrich, D. Nestler, H. Niehoff, P. Wust, B. Thiesen, H. Orawa, V. Budach, A. Jordan, J. Neuro-Oncol. 103 (2011) 317–324.
[5] K. Maier-Hauff, R. Rothe, R. Scholz, U. Gneveckow, P. Wust, B. Thiesen, A. Feussner, A. von Deimling, N. Waldoefner, R. Felix, A. Jordan, J. Neuro-Oncol. 81 (2007) 53–60.
[6] L.H. Reddy, J.L. Arias, J. Nicolas, P. Couvreur, Chem. Rev. 112 (2012) 5818–5878.
[7] M. Wankhede, A. Bouras, M. Kaluzova, C.G. Hadjipanayis, Expert. Rev. Clin. Pharmacol. 5 (2012) 173–186.
[8] J.B. Li, Y. Qu, J. Ren, W.Z. Yuan, D.L. Shi, Nanotechnology 23 (2012) 505706.
[9] D.H. Kim, E.A. Rozhkova, I.V. Ulasov, S.D. Bader, T. Rajh, M.S. Lesniak, V. Novosad, Nat. Mater. 9 (2010) 165–171.
[10] E. Amstad, J. Kohlbrecher, E. Muller, T. Schweizer, M. Textor, E. Reimhult, Nano Lett. 11 (2011) 1664–1670.
[11] V. Nandwana, M. De, S. Chu, M. Jaiswal, M. Rotz, T.J. Meade, V.P. Dravid, Cancer Treat. Res. 166 (2015) 51–83.
[12] C.R. Thomas, D.P. Ferris, J.H. Lee, E. Choi, M.H. Cho, E.S. Kim, J.F. Stoddart, J.S. Shin, J. Cheon, J.I. Zink, J. Am. Chem. Soc. 132 (2010) 10623–10625.
[13] J. Dobson, Nat. Nanotechnol. 3 (2008) 139–143.
[14] S. Hughes, S. McBain, J. Dobson, A.J. El Haj, J. R. Soc. Interface 5 (2008) 855–863.
[15] C. Sanchez, D. El Hajj Diab, V. Connord, P. Clerc, E. Meunier, B. Pipy, B. Payre, R.P. Tan, M. Gougeon, J. Carrey, V. Gigoux, D. Fourmy, ACS Nano 8 (2014) 1350–1363.
[16] X. Jia, L. Jia, Curr. Drug Metab. 13 (2012) 1119–1122.
[17] L. Ma, X. Zou, W. Chen, J. Biomed. Nanotechnol. 10 (2014) 1501–1508.
[18] Y. Svenskaya, B. Parakhonskiy, A. Haase, V. Atkin, E. Lukyanets, D. Gorin, R. Antolini, Biophys. Chem. 182 (2013) 11–15.
[19] E.A. Vitol, V. Novosad, E.A. Rozhkova, IEEE Trans Magn 48 (2012) 3269–3274.
[20] A. Singh, S.K. Sahoo, Drug Discov. Today 19 (2014) 474–481.
[21] F. Zhang, G.B. Braun, A. Pallaoro, Y. Zhang, Y. Shi, D. Cui, M. Moskovits, D. Zhao, G.D. Stucky, Nano Lett. 12 (2012) 61–67.
[22] M.H. Cho, E.J. Lee, M. Son, J.H. Lee, D. Yoo, J.W. Kim, S.W. Park, J.S. Shin, J. Cheon, Nat. Mater. 11 (2012) 1038–1043.
[23] E.M. Zhang, M.F. Kircher, M. Koch, L. Eliasson, S.N. Goldberg, E. Renstrom, ACS Nano 8 (2014) 3192–3201.
[24] Q.T. Ostrom, H. Gittleman, P. Farah, A. Ondracek, Y. Chen, Y. Wolinsky, N.E. Stroup, C. Kruchko, J.S. Barnholtz-Sloan, Neuro-Oncology 15 (Suppl. 2) (2013) ii1–i56.
[25] A.U. Ahmed, M.A. Tyler, B. Thaci, N.G. Alexiades, Y. Han, I.V. Ulasov, M.S. Lesniak, Mol. Pharm. 8 (2011) 1559–1572.
[26] R.P. Cowburn, D.K. Koltsov, A.O. Adeyeye, M.E. Welland, D.M. Tricker, Phys. Rev. Lett. 83 (1999) 1042–1045.
[27] S. Leulmi, H. Joisten, T. Dietsch, C. Iss, M. Morcrette, S. Auffret, P. Sabon, B. Dieny, Appl. Phys. Lett. 103 (2013) 132412.
[28] M. Domenech, I. Marrero-Berrios, M. Torres-Lugo, C. Rinaldi, ACS Nano 7 (2013) 5091–5101.
[29] G.T. Williams, Cell 65 (1991) 1097–1098.
[30] N. Hartung, S. Mollard, D. Barbolosi, A. Benabdallah, G. Chapuisat, G. Henry, S. Giacometti, A. Iliadis, J. Ciccolini, C. Faivre, F. Hubert, Cancer Res. 74 (2014) 6397–6407.
[31] M.M. Gottesman, T. Fojo, S.E. Bates, Nat. Rev. Cancer 2 (2002) 48–58.
[32] D. Yoo, H. Jeong, S.H. Noh, J.H. Lee, J. Cheon, Angew. Chem. Int. Ed. 52 (2013) 13047–13051.
[33] R. Ivkov, S.J. DeNardo, W. Daum, A.R. Foreman, R.C. Goldstein, V.S. Nemkov, G.L. DeNardo, Clin. Cancer Res. 11 (2005) 7093s–7103s.